ments of the energy level and lifetime of the electron in state 1.

ACKNOWLEDGMENTS

We are indebted to M. Kuhn, R. C. Vehse, and H. W. Verleur for supplying p-n junctions and to H. G. White and A. M. Sergent for fabricating p-n junctions used in these experiments. We thank R. Z. Bachrach, J. S. Jayson, J. D. Wiley, and J. J. Hopfield for stimulating discussions.

*Present address: Imaging Science and Engineering Laboratory, Tokyo Institute of Technology, Tokyo, Japan.

[1]H. Kukimoto, C. H. Henry, and F. R. Merritt, preceding paper, Phys. Rev. B 7, 2486 (1973).

[2]S. F. Nygren (private communication).

[3]D. F. Nelson, J. D. Cuthbert, P. J. Dean, and D. G. Thomas, Phys. Rev. Letters 17, 1262 (1966).

[4]P. J. Dean, R. A. Faulkner, S. Kimura, and M. Ilegems, Phys. Rev. B 4, 1926 (1971).

[5]P. J. Dean and C. H. Henry, Phys. Rev. 176, 928 (1968).

[6]J. S. Jayson, R. Z. Bachrach, P. D. Dapkus, and N. E. Shumaker (unpublished).

[7]P. J. Dean, C. H. Henry, and C. J. Frosch, Phys. Rev. 168, 812 (1968).

[8]R. N. Bhargava, Phys. Rev. B 2, 387 (1970).

[9]J. M. Dishman, Phys. Rev. B 3, 2588 (1971).

PHYSICAL REVIEW B VOLUME 7, NUMBER 6 15 MARCH 1973

Infrared Absorption of Localized Longitudinal-Optical Phonons

A. S. Barker, Jr.

Bell Laboratories, Murray Hill, New Jersey 07974

(Received 29 September 1972)

A new type of localized vibrational mode is shown to occur near donors and acceptors in polar semiconductors. In general, the mode appears in a solid with infrared-active lattice vibrations when an impurity center with appropriate electronic transition energies is introduced by doping. The polarizability of the center perturbs the dielectric function locally, shifting the longitudinal-optic phonon. Infrared-reflection data showing the new localized mode are presented for GaP and GaAs. A macroscopic Clausius–Mosotti-type theory is developed for the effective dielectric function of the solid including the spheres. This theory yields good fits to the Raman data of Dean *et al.* and to the present infrared data.

I. INTRODUCTION

Though localized vibrational modes have been studied experimentally for only ten years, a great deal of information has been accumulated for modes in almost every type of crystal system. The most common situation which leads to a localized mode occurs when one of the host atoms of a crystal is replaced by an impurity atom of ligher mass.[1,2] With this replacement there is usually a new vibrational mode of the crystal with frequency above that of all host-lattice modes, and whose eigenvector has most of its amplitude on the impurity atom.[2] The model for such a mode is microscopic, involving the mass change at the impurity site and possibly force-constant changes for the bonds linking the impurity to the neighboring host atoms. In contrast to this microscopic type of local mode, this paper presents a theoretical and experimental study of a localized mode involving a group of host atoms near an impurity. The group of atoms is influenced by the presence of an impurity because of its special electronic properties.

Dean *et al.* were the first to observe this new type of localized vibrational mode. They observed the mode in the Raman spectrum of donor impurities in gallium phosphide.[3] The same modes have recently been detected by infrared techniques.[4] In the present paper we study the absorption of these modes by infrared reflectivity and present a macroscopic dielectric theory for their frequency and line shape. In addition, the Raman scattering strength is derived from the theory and compared with the Raman spectra. For either the infrared or Raman activity of this type of localized mode we adopt a point of view quite different from that of the microscopic defect model. As an example consider the donor sulfur (S) replacing a P ion in GaP. Such a replacement might lead to a localized mode of the microscopic type though it has not yet been observed. Such a mode need not concern us further. If the GaP crystal is cooled, the extra electron of the donor is no longer thermally excited into the conduction band. It resides in the 1S level of the donor. This bound electron is polarizable and thus changes the dielectric function of the medium in its vicinity. It is this extra polarizability, which we describe mac-

roscopically, which causes the new localized mode. We recall that the bulk longitudinal-optic (LO) phonon occurs at the frequency ω_{LO} where the dielectric function $\epsilon(\omega)$ of GaP is zero. Near the bound electron $\epsilon(\omega)$ is locally perturbed and has its zero at a new frequency. This situation leads to new modes which are localized or bound to the donor atom.[3,4] For all of the cases studied to date these localized modes lie just below ω_{LO} regardless of the donor mass. This behavior is in distinct contrast to simple local-mode theories of the microscopic type. Such theories would predict a strong dependence on mass with some of the modes occurring above ω_{LO}. In Sec. II the macroscopic theory of the new localized modes is given in detail. Section III gives the experimental details. In Sec. IV the results and comparisons with the macroscopic theory are presented.

II. DIELECTRIC SPHERE MODEL

A. Effective Dielectric Function

Figure 1 shows the model to be considered. A bulk medium with dielectric function $\epsilon_m(\omega)$ contains spherical regions which have a different dielectric function $\epsilon_s(\omega)$. In the case of donors in GaP we can take $\epsilon_s(\omega)$ to be $\epsilon_m(\omega)$ plus a term due to the bound electron $\epsilon_e(\omega)$. The derivation below is perfectly general and does not depend on the exact form of ϵ_s. In addition to ϵ_m and ϵ_s, we specify the radius r_s of the spheres and the volume density of spheres N_s. The product $N_s r_s^3$ is assumed to be much less than 1 so that the spheres do not touch or overlap.

The actual geometrical distribution of spheres will be needed in evaluating the local field. We will use the Lorentz local field which is appropriate for the random distribution which should obtain in most cases of interest. Two other assumptions are needed regarding r_s and N_s of the spheres. Since we are using macroscopic dielectric functions each dielectric sphere should contain many ions. On the other hand, we wish to describe the entire solid by an effective dielectric function which includes the effects of the spheres. This feature requires that in the frequency region of interest (where resonances or bound modes occur), the sphere radius and the sphere separation must be much less than a wavelength λ of the radiation field in the dielectric. We may list all the above inequalities as

$$a_0 \ll r_s \ll 3(1/N_s)^{1/2} \ll \lambda \,, \tag{1}$$

where a_0 is the primitive cell length.[5]

To construct the dielectric function of the solid shown in Fig. 1 we first note that only relative dielectric functions are important in problems of this type.[6] Figure 1 then goes over to Fig. 2 where spheres of dielectric function $\epsilon = \epsilon_s/\epsilon_m$ reside in a medium with dielectric function 1.

Treating the spheres in Fig. 2 as a gas of polarizable molecules we use the standard result for the dielectric function of such a gas,

$$\epsilon_{gas} = 1 + \frac{4\pi N_s \alpha}{1 - \frac{4}{3}\pi N_s \alpha} \,, \tag{2}$$

where we have made use of the Lorentz field and α is the polarizability of each sphere arising from its dipole moment p induced by the local field E_{loc}:

$$\alpha = p/E_{loc} \,. \tag{3}$$

Since the spheres have dielectric function ϵ we can evaluate their polarization P and hence their dipole moment directly:

$$P = \frac{\epsilon - 1}{4\pi}\left(E_{loc} - \tfrac{4}{3}\pi P\right) \,. \tag{4}$$

The second term in the parentheses is the depolarizing field in a sphere. Since

$$p = P\tfrac{4}{3}\pi r_s^3 \tag{5}$$

we find from Eqs. (3)–(5) that

$$4\pi N_s \alpha = N_s(\tfrac{4}{3}\pi r_s^3)[3(\epsilon - 1)/(\epsilon + 2)] \,. \tag{6}$$

The first two factors on the right-hand side define a dimensionless filling factor

$$f = N_s \tfrac{4}{3}\pi r_s^3 \,. \tag{7}$$

Substitution of Eq. (6) in Eq. (2) gives the effective dielectric function of the system as

$$\epsilon_{gas} = 1 + \frac{3(\epsilon - 1)f}{\epsilon + 2 - (\epsilon - 1)f} \,. \tag{8}$$

For $f \to 0$ (no spheres), ϵ_{gas} reverts to 1 as expected. For small but finite f the medium has a

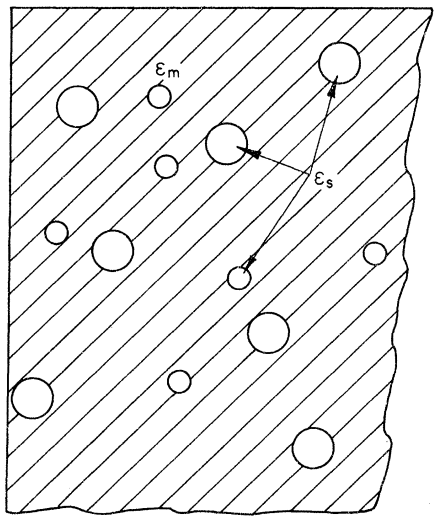

FIG. 1. Model of a solid with dielectric constant ϵ_m and embedded spheres with dielectric constant ϵ_s.

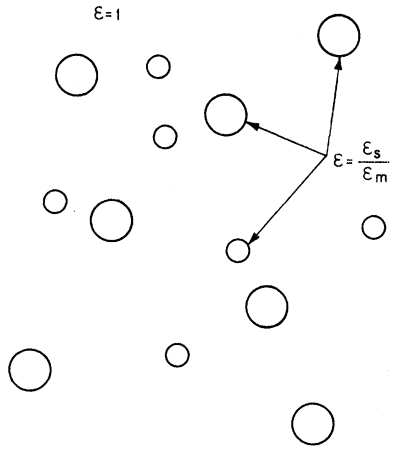

FIG. 2. Simplified model with spheres having the reduced dielectric constant ϵ in a vacuum.

transverse-optic (TO) mode at the pole[7] of ϵ_{gas} given by

$$\epsilon = -2 - 3f , \tag{9}$$

and a LO mode at the zero given by

$$\epsilon = -2 + 6f . \tag{10}$$

In Eqs. (9) and (10) we have dropped terms of order f^2. In the small f limit these two modes coalesce to the frequency where[8]

$$\epsilon = -2 . \tag{11}$$

This is the usual resonance condition for an isolated sphere in a vacuum.[9] The resonance in ϵ_{gas} given by Eq. (11) is in fact a localized mode bound to the sphere since at the frequency where Eq. (11) obtains, a vanishingly small driving field causes a polarization field which is a sum of classical dipole fields each localized on a sphere. Figure 3 shows this new mode for a region of the dielectric much smaller than a wavelength.

To obtain the general result which applies to Fig. 1, Eq. (8) is multiplied through by ϵ_m to remove the relative dielectric function ϵ. The result is the effective dielectric function for spheres embedded in a solid[10]:

$$\epsilon_{eff} = \epsilon_m + \frac{3\epsilon_m(\epsilon_s - \epsilon_m)f}{\epsilon_s + 2\epsilon_m - (\epsilon_s - \epsilon_m)f} . \tag{12}$$

Examination of Eq. (12) shows that if the spheres are absent ($f = 0$) the dielectric function reverts to ϵ_m as expected. For finite but small f, ϵ_{eff} has transverse modes at the poles of ϵ_m (as it has for $f = 0$) and also near the frequencies where

$$\epsilon_s = -2\epsilon_m . \tag{13}$$

Condition (13), which has replaced Eq. (11), again defines localized resonances centered on the spheres. For the simple model of donors in GaP described below, Eq. (13) has two solutions at two distinct frequencies, both localized, one of which is phononlike and one electronlike.

B. Model Calculations

To illustrate the localized phonon resonance the effective dielectric function ϵ_{eff} may be calculated using assumed forms for ϵ_s and ϵ_m in Eq. (12) above. Taking the case of donors in GaP we choose ϵ_m to be the dielectric function of insulating (undoped) GaP. At low temperatures the donor electrons will reside in their lowest energy level which is localized on the donor impurity. It is known that the radius of a donor is about 10 Å. Within a sphere of this radius there are 104 Ga-P ion pairs and the first part of the inequality [Eq. (1)] is fairly well satisfied. At low temperatures the electrons can be described by a dielectric function within the spheres (ϵ_s) which is the sum of ϵ_m (due to the Ga-P ions) plus a resonance corresponding to the allowed donor transition $1S$-$2P$. For the present calculation we replace all higher-

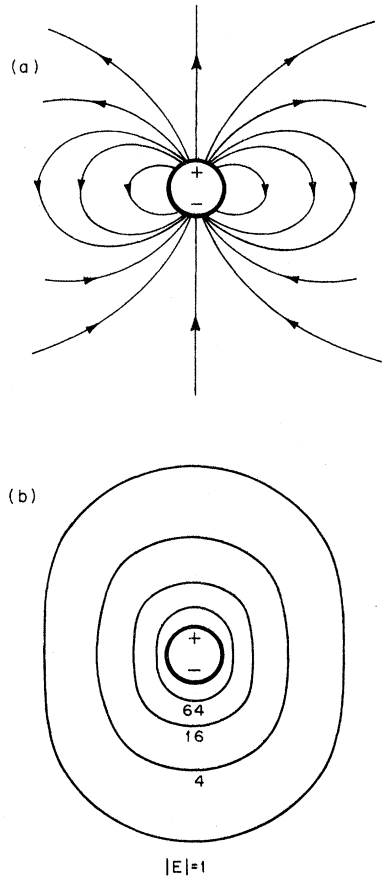

FIG. 3. Resonance in the vicinity of one of the dielectric spheres. In (a) the electric field lines are shown while in (b) the locus of points of constant electric field are shown as solid curves.

lying electronic transitions of the donor by a frequency-independent polarizability which gives a dielectric constant ϵ_∞^{el}. In summary, our assumed forms are

$$\epsilon_m = \epsilon_\infty + \frac{S_0\omega_0^2}{\omega_0^2 - \omega^2 - i\omega\gamma_0} \tag{14}$$

for the medium and

$$\epsilon_s = \epsilon_{el} + \epsilon_m = \epsilon_\infty^{el} + \frac{S_1\omega_1^2}{\omega_1^2 - \omega^2 - i\omega\gamma_1} + \epsilon_m \tag{15}$$

for the spheres.

In Table I we list some values of the parameters in Eqs. (14) and (15). For ϵ_m we have chosen the values typical of GaP, with the TO mode at 367 cm^{-1}. The second line in the table describes the electronic resonance ϵ_{el}. For this term we have put the resonance ω_1 ($1S-2P$ transition) at 500 cm^{-1} or 62 meV. Figure 4 shows the real parts of the dielectric function. In Fig. 4(a) the GaP resonance is seen with its strong resonant dispersion at 367 cm^{-1}. Figure 4(b) shows the sphere dielectric function ϵ_s. This function has the GaP resonance plus the electron resonance at 500 cm^{-1}. Equation (12) can now be calculated once we choose the concentration of spheres specified by the dimensionless filling factor f. For $f=0.10$, ϵ_{eff} shows the two resonances near 367 and 500 cm^{-1} plus a new resonance near 398 cm^{-1} [see Fig. 4(c)]. This new resonance is the localized or bound LO phonon. It occurs just below ω_{LO} at the frequency given by Eq. (13). Because of the damping included in Eqs. (14) and (15) the solutions of Eq. (13) are complex, leading to a finite width for the resonance.

TABLE I. Dielectric parameters for model calculations. $f=0.1$ used in all calculations.

	Frequency ω_i (cm^{-1})	Strength S_i	Linewidth γ_i (cm^{-1})	High-ω limit ϵ_∞
	Case 1 (Figs. 5 and 6)			
ϵ_m	367	1.96	0.73	9.1
ϵ_{el}	500	0.3	1.0	7.0
	Case 2 (Figs. 7 and 8)			
ϵ_m	367	1.96	0.73	9.1
ϵ_{el}	400	1.0	0.8	7.0

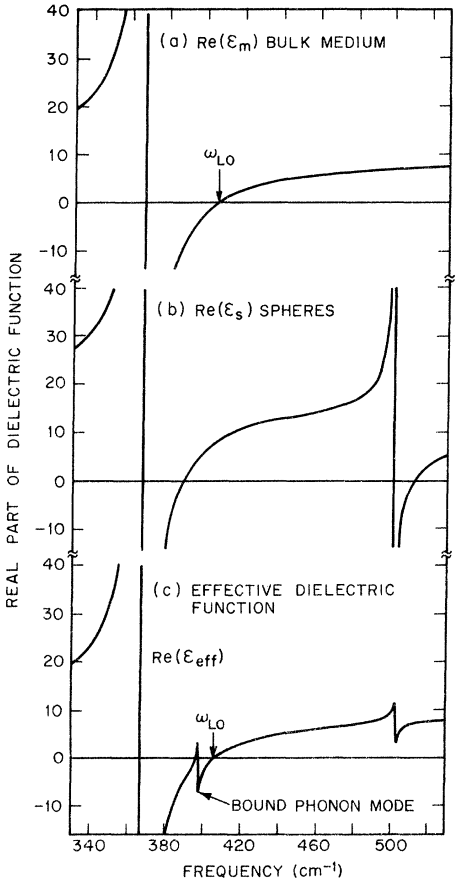

FIG. 4. Dielectric function for a model calculation of donor spheres in GaP. In (a) the ϵ_m for bulk GaP is shown. In (b) ϵ_s for the spheres which include ϵ_m and a resonance at 500 cm^{-1} is plotted. The parameters are given in Table I. (c) The real part of the effective dielectric function for the system. Note the new resonance near 398 cm^{-1} and the electron resonance shifted slightly above 500 cm^{-1}.

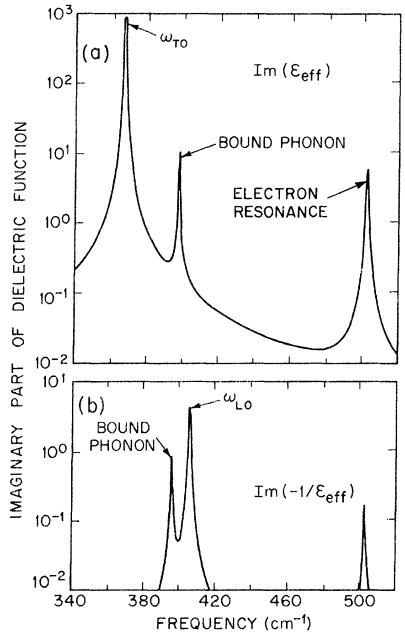

FIG. 5. Imaginary part of the effective dielectric function for the model shown in Fig. 4. There are TO peaks near the poles of ϵ_{eff} shown in (a). The LO modes correspond to the zeros in ϵ_{eff} and occur as peaks for the plot shown in (b).

In Fig. 5 the mode shapes of the resonances are examined by plotting the imaginary parts of the dielectric function. $\mathrm{Im}(\epsilon_{eff})$ reveals the transverse-mode shape and $\mathrm{Im}(-1/\epsilon_{eff})$ gives the longitudinal-mode shape.[7] Figure 5 shows transverse- and longitudinal-mode peaks near 398 cm^{-1}. The TO–LO splitting of these bound phonon peaks is quite small for the parameters chosen (less than 2 cm^{-1}). The splitting must be finite for finite f and the modes must be included in the generalized Lyddane–Sachs–Teller relation[11] along with the other polar modes to give a correct description of the macroscopic dielectric function of the crystal. The resonance in ϵ_{eff} near 398 cm^{-1} also causes polariton modes to be connected with the localized resonances. The polariton effects will be weak for the example chosen here but in any case can be evaluated using ϵ_{eff} in the polariton dispersion curve formula.

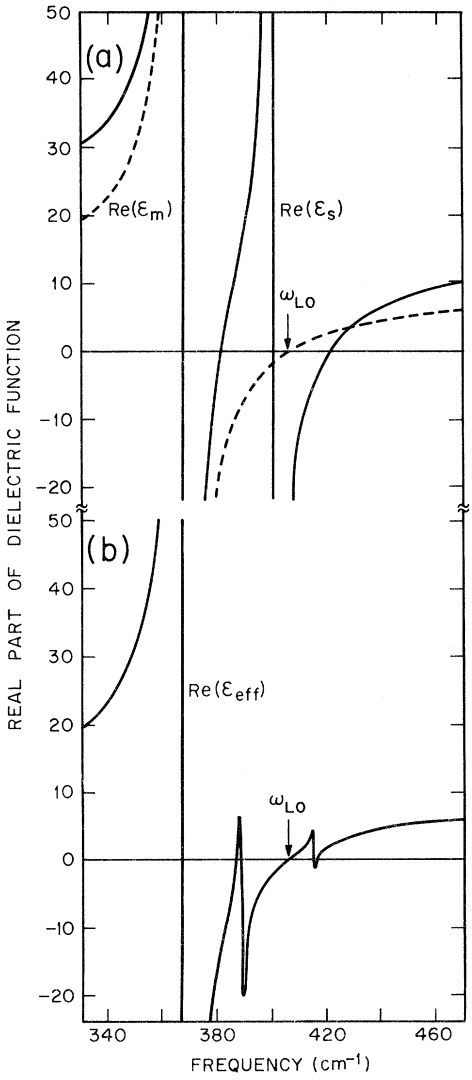

FIG. 6. Dielectric function for a model of donor spheres with the electron resonance very near the LO phonon frequency at 404 cm^{-1}. In (a) the dielectric functions for the medium and the spheres are shown separately. The parameters are given in Table I. In (b) the interacting system dielectric function ϵ_{eff} shows two new resonances near 387 and 416 cm^{-1}.

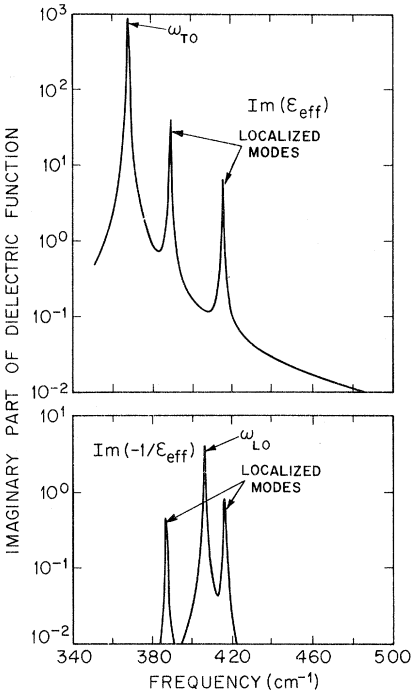

FIG. 7. Imaginary part of the effective dielectric function shown in Fig. 6(b). The new resonances caused by the electronic transition are marked as localized modes. The strongest features in the spectra are still the bulk phonons of GaP labeled ω_{TO} and ω_{LO}.

The area under the bound LO phonon peak [either $\mathrm{Im}(\epsilon_{eff})$ or $\mathrm{Im}(-1/\epsilon_{eff})$] is proportional to f in the low-concentration limit. The peaks near 500 cm^{-1} are also proportional to f. These latter peaks are localized resonances connected with the electronic transition which has been idealized to the one resonance oscillator form used for ϵ_{el} in our example. A calculation using equations of motion shows that the resonance at 398 cm^{-1} has an eigenvector which is predominately phononlike, while the resonance near 500 cm^{-1} is predominately electronlike. If the nonintereacting systems are closer to resonance (i.e., if $\omega_1 \to \omega_0$), strong mixing occurs. In this situation both localized modes have mixed character, containing roughly equal parts of electron and phonon amplitude.

It is probably worthwhile at this point to summarize the physical effect which is causing the new localized mode. Neglecting imaginary parts, Eq. (13) shows that the sphere must have a dielectric

constant which is -2 times the dielectric constant of the medium. This condition results in self-sustained oscillations in the following way. Polarization of a sphere creates dipole fields which cause all nearby spheres to polarize. These spheres in turn give dipole fields which have exactly the right magnitude and direction [when Eq. (13) holds] to drive the polarization we postulated in the first sphere. If the sphere contains some polarizable entity (e.g., a bound electron or hole) so that ϵ_s is positive, then, since ϵ_m passes through zero at ω_{LO} and is negative just below, this region below ω_{LO} is the place where we can expect Eq. (13) to be satisfied. If ϵ_s is negative, then Eq. (13) may be satisfied just above ω_{LO} where ϵ_m is positive.

Figure 6 shows a case where ϵ_s is negative near ω_{LO}. Table I (lower part) gives the parameters used. There are two bound resonances, one just above ω_{LO} and the second just below ω_{LO}. Both have mixed electron and phonon character resulting from the near degeneracy of the uncoupled systems. Figure 7 shows the imaginary parts of the effective dielectric function to illustrate the mode shape. This example of nearly degenerate resonances may be important in polar semiconductors since the binding energies of some donors (or acceptors) in certain cases are very close to the polar phonon frequency. For both cases discussed above (Figs. 5 and 7), the bound resonances have amplitudes localized about the spheres and have the characteristic dipole field pattern given in Fig. 3. Because the resonance condition arises from

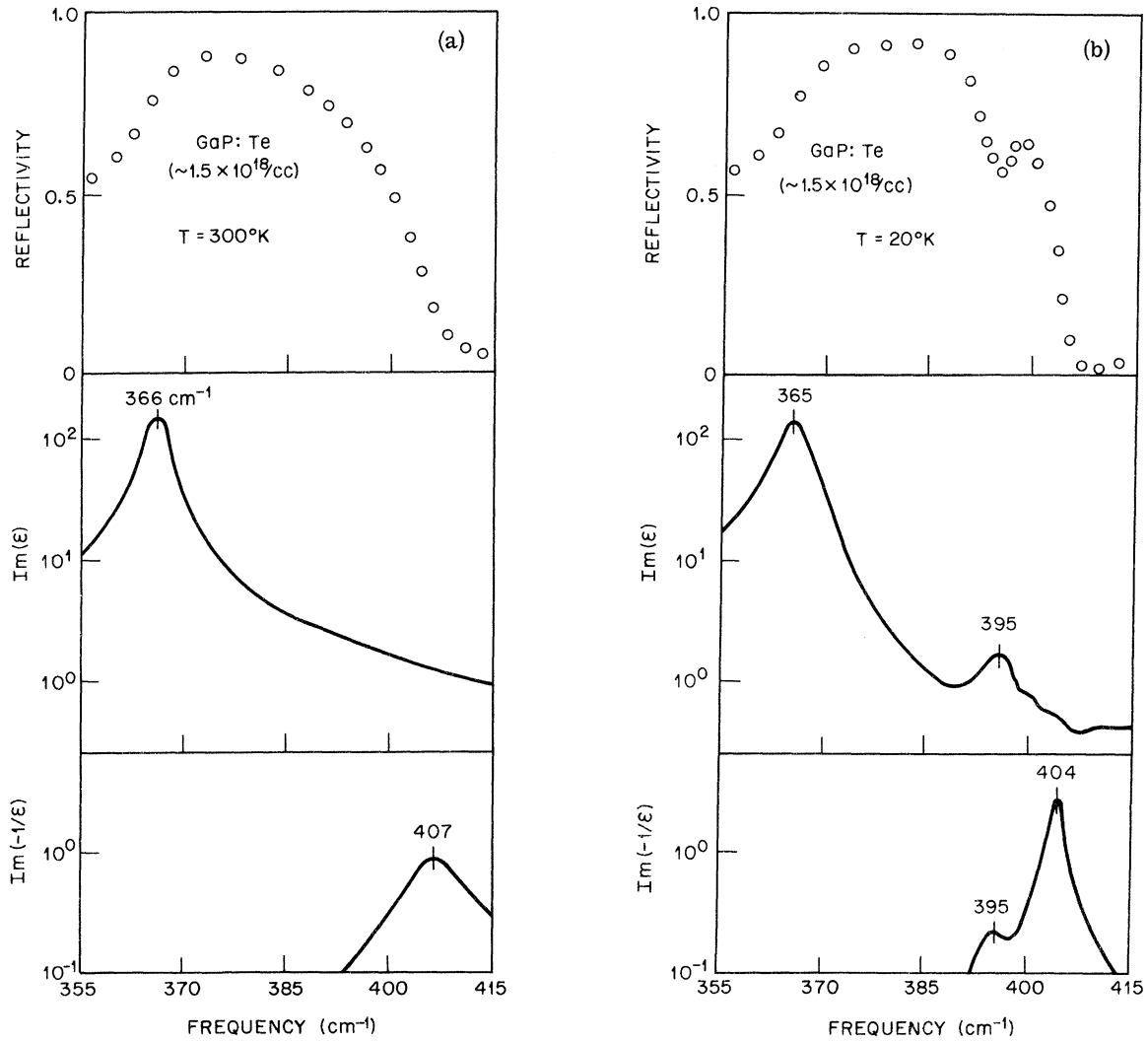

FIG. 8. (a) Infrared data at 300 K for GaP doped with tellurium. The top graph shows the reflectivity spectrum and the lower graphs the dielectric functions obtained by a Kramers–Kronig analysis of the reflectivity. (b) Infrared data at 20 K for the sample of (a). The new localized mode appears at 395 cm^{-1}. It reveals itself clearly in both the $\mathrm{Im}(\epsilon)$ and $\mathrm{Im}(-1/\epsilon)$ spectra.

matching solutions to Maxwell's equations it may be seen that this new type of local mode is not connected with the mass-defect model[2] and may occur above or within the phonon continuum. The linewidth of the mode is described by Eq. (12). In these model calculations the damping is controlled entirely by γ_0 and γ_1. For the case shown in Figs. 4 and 5 where the electron resonance is well removed to higher frequencies, γ_0 dominates in Eq. (12). In this case the localized mode has the same width as the LO phonon.

III. EXPERIMENTAL WORK AND ANALYSIS

Crystals of GaP doped with either a donor or acceptor species were cut and polished by standard metallographic techniques to obtain a flat surface. The orientation and shape of most samples yielded a (111) plane with a surface area of at least 1×5 mm. Reflection spectra were measured at room temperature and at liquid-hydrogen temperature (20 K) in the infrared range 285–1000 cm^{-1} (10–35-μ wavelength). The general method used and a description of the spectrometer have been given earlier.[12] Figure 8 shows the reflectivity of GaP doped with the donor tellurium. These data have been analyzed by a Kramers–Kronig integral transform to obtain the optical constants.[12] In the lower part of Fig. 8(a) the imaginary parts of the dielectric function $\mathrm{Im}(\epsilon)$ and of the reciprocal dielectric function $\mathrm{Im}(-1/\epsilon)$ are plotted. Peaks in $\mathrm{Im}(\epsilon)$ correspond to TO modes and peaks in $\mathrm{Im}(-1/\epsilon)$ to LO modes. At room temperature $\mathrm{Im}(\epsilon)$ shows a strong peak at 366 cm^{-1} due to the infrared-active phonon. This peak has been well documented in earlier infrared and Raman spectra.[13] $\mathrm{Im}(-1/\epsilon)$ shows an LO mode at 407 cm^{-1}. In insulating GaP this LO peak is sharper and occurs at 403 cm^{-1}. The broadening and shift observed here are due to the free electrons associated with the ionized Te donors.

Figure 8(b) shows the reflectivity on cooling to 20 K. A new dip occurs near 395 cm^{-1}. The Kramers–Kronig analysis of these data shows the main TO and LO peaks as before plus a weaker mode at 395 cm^{-1} whose TO-LO separation cannot be resolved. At the same time the broadening and shift of the LO (seen at 300 K) have been reduced since the free electrons are almost completely "frozen out" at 20 K. The peak at 395 cm^{-1} is the localized or bound LO phonon. Figure 9 shows the low-temperature spectra for GaP doped with Se. The localized LO phonon here occurs at 397.5 cm^{-1}. In the $\mathrm{Im}(-1/\epsilon)$ spectrum this peak is not clearly resolvable unless the LO mode background is removed by subtraction.

In Fig. 10 the spectrum of GaP doped with Sn is shown. The spectrum at 300 K shows the plasmon shifted LO due to the presence of 7×10^{17} cm^{-3} free

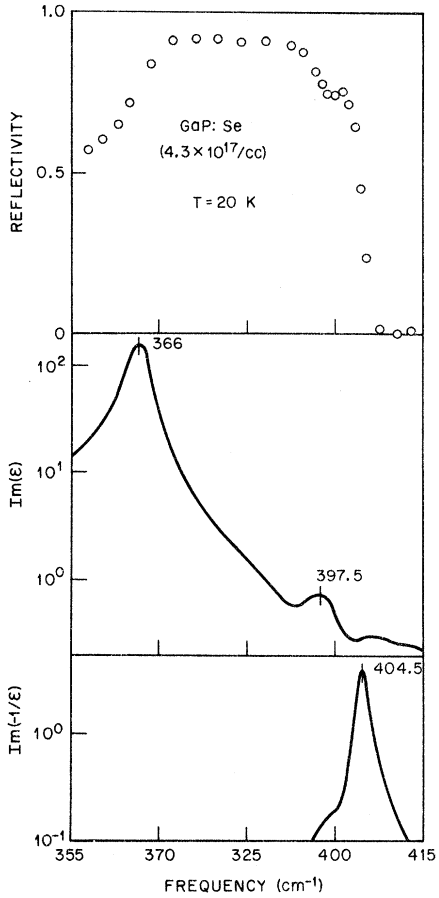

FIG. 9. Infrared data for GaP doped with selenium. The localized mode appears at 397.5 cm^{-1}.

electrons. At 20 K the localized phonon appears. After these spectra had been recorded the crystal was copper-diffused to compensate the crystal. The lowest curve in Fig. 10 shows the resulting low-temperature spectrum. The bound phonon peak is no longer present even though the Sn impurities have not been removed. Figures 11 and 12 show results for S and Si donors in GaP. Many other spectra for various dopants in GaP and GaAs were recorded. Table II lists the crystals studied and shows the binding energies together with some pertinent comments.

IV. DISCUSSION

A. Model Fits to Infrared Spectra

Figures 8–12 show subsidiary peaks near the bulk LO phonon mode in GaP. These peaks range from 7 to 12 cm^{-1} below the LO phonon depending on the donor impurities. These are the bound or localized LO phonon modes. The peaks are qualitatively similar to the spectrum of Fig. 5 for the localized LO mode using the macroscopic model.

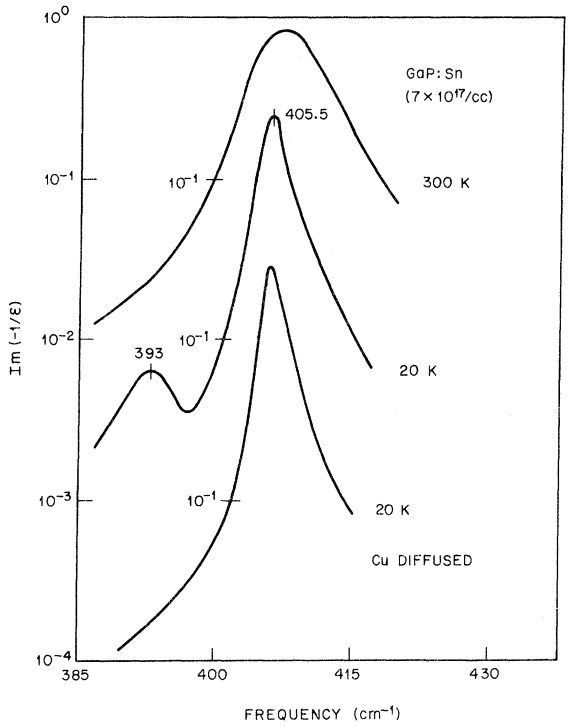

FIG. 10. Infrared data for GaP doped with tin. The $\mathrm{Im}(-1/\epsilon)$ spectrum at 300 K shows only the free-electron effects on ω_{LO}. On cooling the localized mode appears at 393 cm^{-1}. This sample was then Cu diffused to remove the electrons from the tin donors and a new spectrum taken. The lowest curve shows the absence of the localized mode for this case.

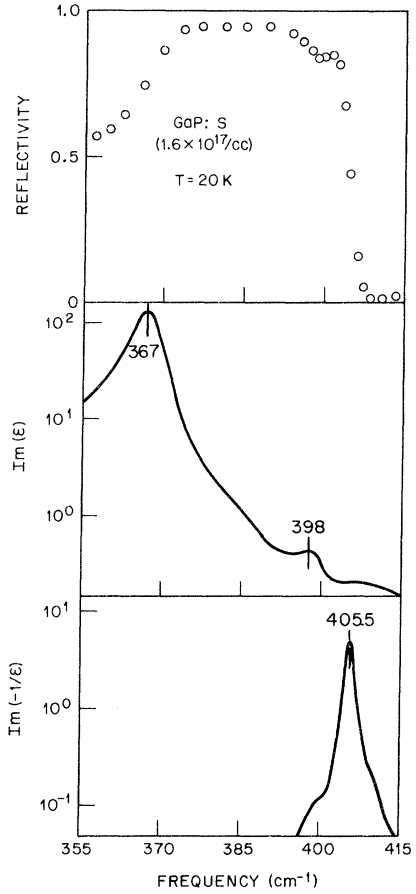

FIG. 11. Infrared spectrum for GaP doped with sulfur. The localized mode appears at 398 cm^{-1} and is weaker than preceding examples because of the low concentration.

Spectra of undoped crystals or doped crystals at 300 K show no such peaks. This fact, together with the lack of a peak for the Cu-compensated sample in Fig. 10, confirms that the peaks are associated with the bound electron at the donor site. All of the donors shown in Figs. 8–12 have a $1S$-$2P$ transition energy greater than $\hbar\omega_{LO}$. In the region of ω_{LO} this transition causes ϵ_{el} [Eq. (15)] to be positive so that Eq. (13) has a solution at a frequency just below ω_{LO} in agreement with the peaks observed. Equation (12) may be evaluated for various values of ϵ_{el}. Figure 13 shows predicted localized LO phonon frequencies [i.e., the peak in $\mathrm{Im}(-1/\epsilon_{eff})$] evaluated in this way. The five donors studied have been placed on the curve at the correct ordinate. We note that the dielectric sphere which approximated the donor must have a dielectric constant in the range 6.5–14 for these donors.

Figure 14 shows a fit of the macroscopic model to the $\mathrm{Im}(-1/\epsilon)$ spectrum of GaP with Te. The Te donor is described by an oscillator to represent the $1S$-$2P$ transition [cf. Eq. (15)]. The parameters of the fit are given in the figure. The fit is good considering the uncertainties in the experi-

TABLE II. Donor and acceptor binding energies in GaP and GaAs[a].

Element (and site)	E_B[b] (meV)	Remarks
		Donors
S (P)	104.1	Bound LO mode seen in reflectivity
Se (P)	102.0	
Te (P)	89.8	
Si (Ga)	82.1	
Sn (Ga)	65.5	
		Acceptors
Zn (Ga)	64.0	Mode not detected—may be damped
Cd (Ga) in GaAs	30	
Be (Ga)	50	
Mg (Ga)	53.5	
C (P)	48.0	Weak mode 6 cm^{-1} below ω_{LO}
Ge (As) in GaAs	38	Weak mode seen 5 cm^{-1} below ω_{LO}

[a]All impurities are in GaP except for Cd and Ge in GaAs.

[b]Binding energies from M. R. Lorenz, G. D. Pettit, and S. E. Blum, Solid State Commun. 8, 705 (1972); P. J. Dean (private communication).

mental data. The rather broad bulk LO and localized LO peaks require large damping factors in the oscillator expressions. Some of the breadth may be associated with surface strain or damage. This is a problem intrinsic to all surface reflectivity measurements. We will present Raman spectra (taken deep within a GaP: Te sample) below which show smaller linewidths. The linewidth problem will not be discussed further since our main interest is in the strength and frequency of the localized modes. These latter quantities should be quite insensitive to linewidth.

The localized modes associated with all of the donors may be fit to the same or better precision as has been done for the case of Te. The parameters required are similar except that the mode strength (controlled by f) and the mode shift (controlled by the value of ϵ_{el} near the localized mode) must be choosen separately in each case. These two aspects of the fitting are discussed below.

B. Significance of Parameters

The fit of the dielectric sphere model for the case of Te (Fig. 14) requires the value $f = 0.11$.

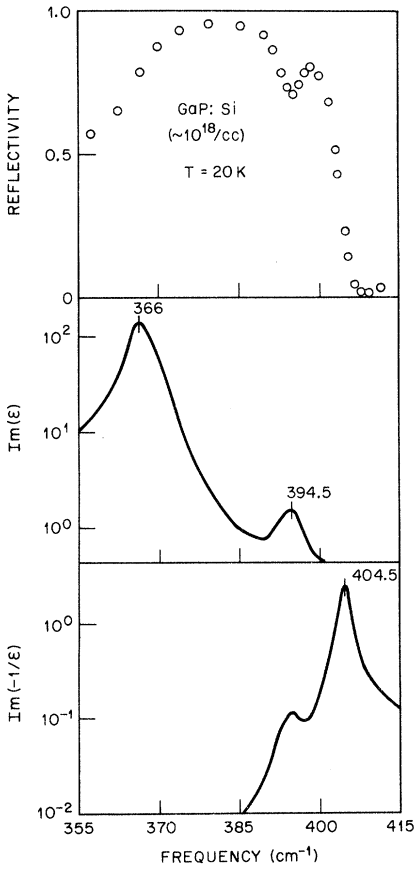

FIG. 12. Infrared spectrum of GaP doped with silicon. The localized mode appears at 394.5 cm^{-1}.

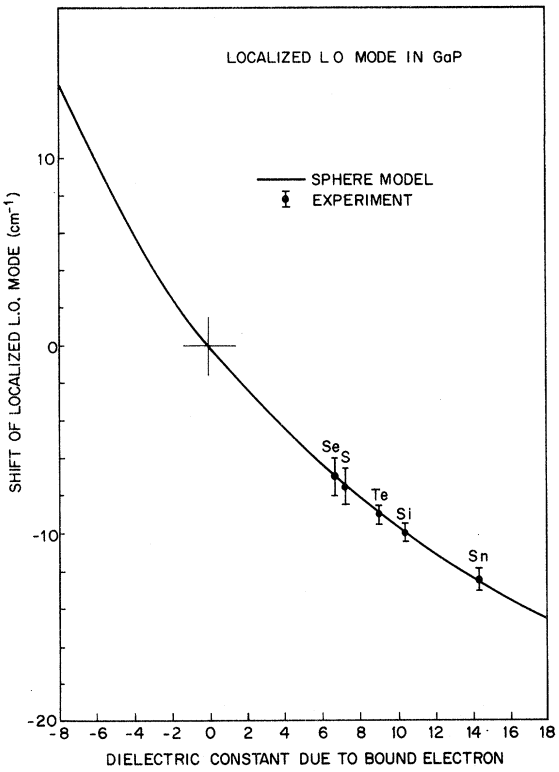

FIG. 13. Calculated shift of the localized mode from the bulk LO phonon. The frequency of localized mode peak in $\mathrm{Im}(\epsilon_{\mathrm{eff}})$ has been calculated for a range of values or ϵ_{el}. The calculation is done with low damping and small concentration ($f < 0.01$). For f appreciably larger than 0.1 the curve becomes more horizontal. The observed modes have been placed on the curve at the correct ordinates.

From Eq. (7) and the concentration given in the figure we derive a sphere radius of $r_s = 26$ Å. This radius appears reasonable. The donor Bohr radius is about $a = 10$ Å; however, only 32% of the probability amplitude for a hydrogenic ground-state wave function lies inside a sphere of this radius. 76% lies within a sphere of radius $2a = 20$ Å, which is in better agreement with the radius derived from the model. In addition, we note that the model is self-consistent in that the derived r_s obeys all three inequalities given in Eq. (1).

A second related measure of mode strength may be defined without fitting the spectra. The integrated strength under the curve $\mathrm{Im}(-1/\epsilon)$ may be evaluated by interpolating and subtracting the background under the localized mode. This strength may then be normalized by dividing by the area under the bulk LO mode. We write

$$A = \frac{\int_{\text{local mode}} \mathrm{Im}(-1/\epsilon)\, d\omega}{\int_{\text{bulk LO mode}} \mathrm{Im}(-1/\epsilon)\, d\omega} \tag{16}$$

for the definition of the normalized strength. In

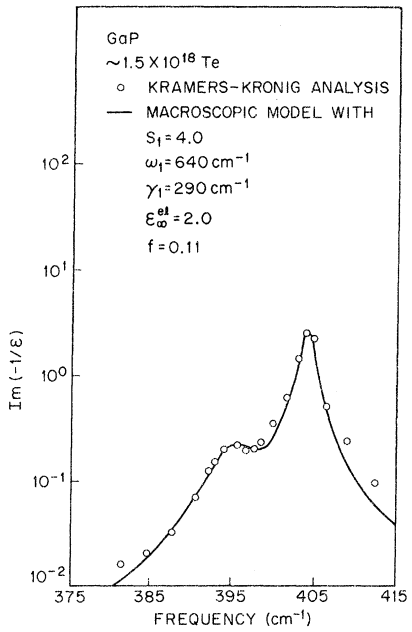

FIG. 14. Fit of the macroscopic sphere model to the infrared data of GaP with Te. The parameters for the donor transition are given in the figure. The GaP phonon mode (ϵ_m) is parametrized as in Table I except that γ_0 has been increased to 2.2 cm^{-1}.

practice the limits of integration are in the 385–451-cm^{-1} range and the procedure has an uncertainty of ± 40% in A for the present infrared data. Figure 15 shows this normalized absorption strength plotted against concentration. Somewhat surprisingly, the points all lie close to a single straight line of unity slope. Manchon has measured the local-mode strength in the case of Raman scattering by the donors Te, S, and Sn.[14] Manchon uses the peak height of the scattering spectrum and normalizes by the height of the bulk LO-mode peak. The results are shown in Fig. 15. While the points are consistently lower, there is again a good indication that a single straight line can describe the local-mode strengths for a variety of donors. A detailed examination of several of the Raman spectra shows that if an integrated Raman cross section is used to define the mode strength, the Raman points are shifted up a factor of 2–3 giving excellent agreement of the two methods. It is obvious that once the calibration (Fig. 15) has been established the local-mode strength can be used as an optical probe of the donor concentration in a semiconductor.[15]

We now turn to the second parameter of importance; the frequency of the localized LO mode. Treating the case of the Te donor, Fig. 13 showed that the dielectric sphere must have a dielectric constant of about 9.0 (near the LO mode) to give the frequency shift observed. Again we make comparison with the quantum theory of the donor. Within the dielectric sphere our model postulates a uniform dielectric constant $\epsilon_{el} + \epsilon_m$ due to the donor and the Ga-P ions. The electronic contribution may be converted to a donor polarizability:

$$\alpha = v(\epsilon_{el} - 1)/4\pi \ . \tag{17}$$

Taking the volume from the preceding strength analysis, we find

$$\alpha = 4.7\times10^{-20} \text{ cm}^3 \quad \text{(GaP experiment)} \tag{18}$$

for the electronic polarizability.

The isolated H atom in vacuum has polarizability[16] $\alpha = 0.67\times10^{-24}$ cm^3. This polarizability is much too small; however, we must allow for the effect of the GaP lattice when using the H-atom treatment of the donor. Using the continuum model[17] for the H atom immersed in a medium of dielectric constant ϵ (independent of frequency), the polarizability is enhanced by the factor ϵ^4. The principle donor transitions for Te in GaP lie in the range 600–4000 cm^{-1}, where the dielectric constant of GaP is approximately 9 with a small amount of dispersion. (It is accidental that the electronic part of ϵ_s is also 9 in the case of Te.) Making the dielectric correction to the free-atom

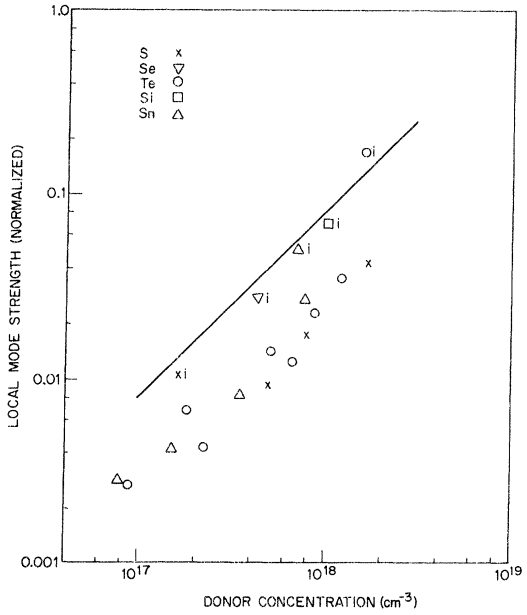

FIG. 15. Strength of localized mode relative to LO mode plotted against donor concentration (see text). The five points labeled i are taken from preceding infrared spectra. The remaining points are taken from Raman data of Manchon. Uncertainties are typically ± 20% in both the concentration and strength measurements except that the infrared strengths have a ± 40% uncertainty. When the Raman points are corrected to give integrated strength then all points lie close to the straight line with unity slope.

result, we obtain

$$\alpha = 0.44\times10^{-20}\ \text{cm}^3 \quad (\text{H atom in } \epsilon = 9)\ . \tag{19}$$

Only order-of-magnitude agreement is obtained in comparing the continuum model with the sphere model. The agreement is much improved if a smaller sphere radius r_s is used in computing v in Eq. (17). A closer comparison of the sphere model must await a detailed quantum theory of the donor states and transition probabilities in polar semiconductors.[17]

C. Raman Spectra

Figure 16 shows the Raman scattering spectrum of a GaP: Te sample taken at low temperature.[14] The bulk LO and the localized LO modes appear very similar to the infrared spectrum of Fig. 14. The lines are somewhat narrower and there is a shift of both lines to higher frequency by 1.5 cm^{-1}. The shift is not significant since it is within the frequency calibration uncertainties of the Raman and infrared spectra. The linewidth effect is probably real; the greater damping being observed in the infrared spectrum taken at the crystal surface. The solid line in Fig. 16 is a fit to the data using the dielectric sphere model. To apply the model to Raman scattering the macroscopic approach is used. The effective dielectric function ϵ_{eff} (derived in Sec. II) is inserted into the standard scattering formulas for bulk GaP. For 90° Stokes scattering the TO and LO scattering formulas are[18]

$$\left(\frac{d^2\sigma}{d\Omega\, d\omega_s}\right)_{\text{trans}} = A[n(\omega)+1]\,\text{Im}(\epsilon_{\text{eff}})\ , \tag{20}$$

$$\left(\frac{d^2\sigma}{d\Omega\, d\omega_s}\right)_{\text{long}} = A[n(\omega)+1]\,(169)\,\text{Im}(-1/\epsilon_{\text{eff}})\ . \tag{21}$$

A is a frequency-independent factor for nonresonant scattering, $n(\omega)+1$ is the usual Stokes factor, and 169 is a numerical factor which arises from the lattice dynamics of GaP. The numerical factor 169 causes the LO-mode scattering to be stronger than the TO-mode scattering near the localized LO mode. The solid curve in Fig. 16 is a plot of the right-hand side of Eq. (21) with A adjusted for a best fit. At the temperature of the Raman experiment (20 K), $n(\omega) \approx 0$ so that in the 390–410-cm^{-1} range the Raman experiment measures the same spectrum $[\text{Im}(-1/\epsilon_{\text{eff}})]$ as that given by the Kramers–Kronig analysis of the infrared spectrum. It is evident from Fig. 16 that once the narrower linewidths have been allowed for, the macroscopic theory gives a good fit to the important features of the Raman spectrum.

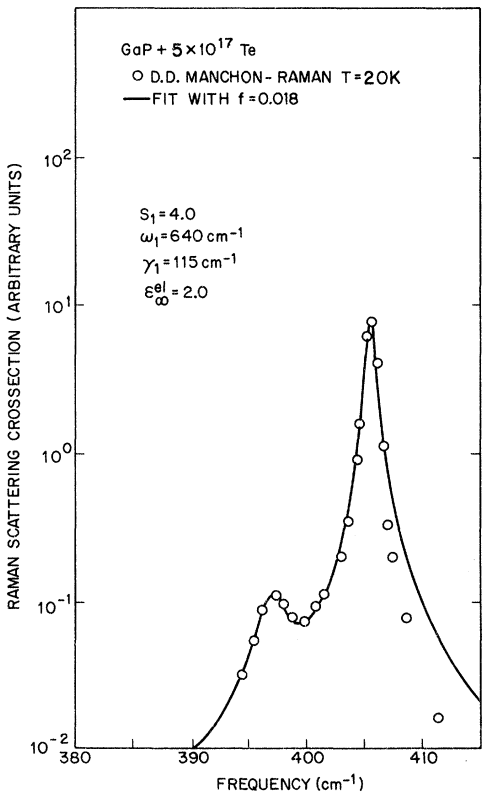

FIG. 16. Fit of the dielectric sphere model to a 90° Raman scattering spectrum of GaP doped with Te. The donor-transition parameters are given in the figure. The GaP phonon-mode parameters are the same as in Table I except that the linewidth has been increased slightly to $\gamma_0 = 0.96\ \text{cm}^{-1}$.

D. Localized LO Modes for Acceptors

The dielectric sphere theory allows the possibility of localized LO modes connected with acceptors in a polar semiconductor. If the acceptor has an optically active transition (e.g., $1S \rightarrow 2P$) with an energy greater than $\hbar\omega_{\text{LO}}$, then the model in Sec. II applies exactly as for the donor and predicts a localized mode below $\hbar\omega_{\text{LO}}$. Figure 13 shows that even if the acceptor (or donor) transition is just below $\hbar\omega_{\text{LO}}$ a localized mode can still be observed; but now it appears on the high-frequency side of $\hbar\omega_{\text{LO}}$. From Table II we note that the binding energies of Zn and Mg acceptors are just above $\hbar\omega_{\text{LO}}$. If the approximate relation $E(1S \rightarrow 2P) \approx \frac{3}{4} E_B$ is used, then these acceptor transitions fall at 390 cm^{-1} (Zn) and 320 cm^{-1} (Mg). Low-temperature reflectivity scans of Zn- and Mg-doped samples show no localized-mode peaks either above or below ω_{LO} (see Fig. 17). We believe that this negative result is due to the large damping of these acceptor transitions and does not reflect any failure of the theory. Figure 18 shows the results of Henry *et al.* for the Raman scattering of a GaP: Zn sample.[19] The broad peak labeled C at 450 cm^{-1} is associated with the presence of zinc acceptors but has not been given a definite assignment. It ap-

pears likely that this peak corresponds to the $1S$-$2P$ transition. There is an indication of this same peak in the $\mathrm{Im}(\epsilon)$ spectrum of Fig. 17. The reflection method is quite insensitive to these relatively low values, however, where $\mathrm{Im}(\epsilon) \ll \mathrm{Re}(\epsilon)$. A broad absorption peak very similar to C is seen in the low-temperature infrared transmission spectrum of zinc-doped GaP.[20] The peak C is the transition which we wish to model by choosing a suitable form for the term ϵ_{el} in Eq. (15). As shown in the lower part of Fig. 18, we choose ϵ_{el} as a broad mode peaked at 390 cm^{-1} and evaluate the dielectric sphere model. The interactions included in the equation for ϵ_{eff} cause a broad absorption band in $\mathrm{Im}(\epsilon_{eff})$ peaked near 450 cm^{-1} [see Fig. 18(c)]. This peak is in agreement with the infrared absorption spectrum.[20] The $\mathrm{Im}(-1/\epsilon_{eff})$ spectrum shows an unresolved shoulder on the low-frequency side of the LO phonon. The unresolved shoulder and the broad peak near 450 cm^{-1} are the localized LO phonons. Because of the near degeneracy of the electronic transition and the

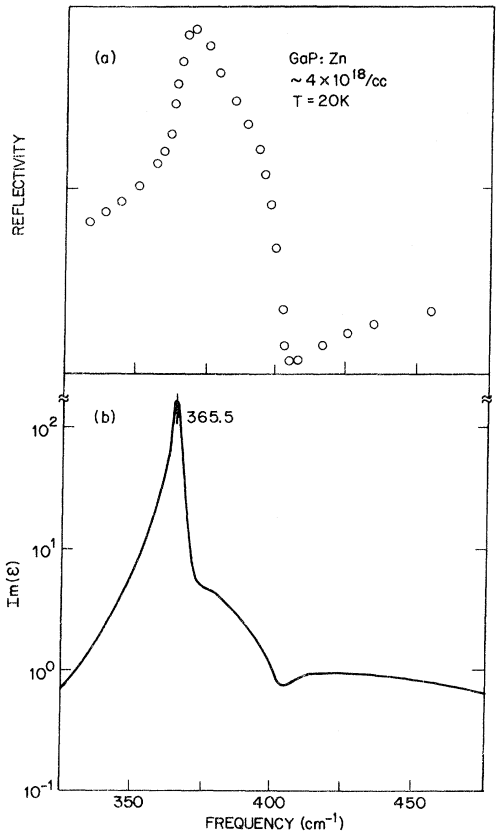

FIG. 17. (a) Low-temperature reflectivity spectrum of GaP doped with zinc. There is a noticeable flattening near 385 cm^{-1} due to the zinc. (b) $\mathrm{Im}(\epsilon)$ spectrum obtained by Kramers–Kronig analysis of the data in (a). Note the broad featureless absorption above 400 cm^{-1}.

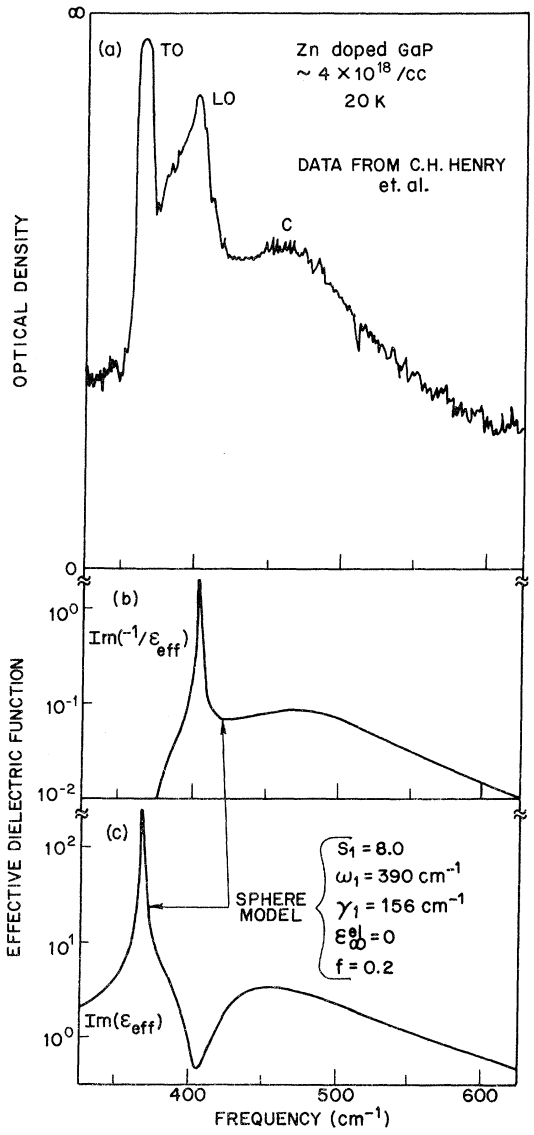

FIG. 18. Spectra for the acceptor zinc in GaP. (a) The low-temperature Raman spectrum from the work of Henry *et al.* The graph is a densitometer trace of a photographically recorded spectrum. Besides the TO and LO peaks there is a broad mode labeled C near 460 cm^{-1}. (b) and (c) are rough fits to (a) using the dielectric sphere model. The zinc transition parameters are given in the figure. The GaP phonon-mode (ϵ_m) parameters are the same as Table I except that the linewidth $\gamma_0 = 2.2$ cm^{-1} has been used.

bulk phonon mode, the interacting system (ϵ_{eff}) is heavily mixed, having phonon and electron amplitude at both resonances. An interesting comparison can be made between the donor Sn and the acceptor Zn. Both have approximately the same binding energy so that it would appear that since Sn causes a sharp localized mode, Zn should also. In fact, it is the damping of the transition which

must be considered as well as E_B. For a fit to the Sn mode (Fig. 14) we find that $\mathrm{Im}(\epsilon_{el}) = 2.5$ at 400 cm^{-1}. For the Zn fits $\mathrm{Im}(\epsilon_{el}) = 20.0$ at 400 cm^{-1}, which again emphasizes the highly damped nature of the Zn transitions.

The Raman scattering cross section is directly related to the calculated spectra ϵ_{eff} by Eqs. (20) and (21). From Fig. 18(a) it is evident that the crystal orientation was not optimized for LO scattering. This fact prevents us from using Eqs. (20) and (21) directly with the factor 169. Reducing this factor to about 100 we note that the addition of $\mathrm{Im}(\epsilon_{\mathrm{eff}}) + 100 \times \mathrm{Im}(-1/\epsilon_{\mathrm{eff}})$ does give an approximate reproduction of the Raman spectrum of Henry *et al.* in the 325–625-cm^{-1} region. In addition, we may calculate the infrared reflectivity for the sphere model used in Fig. 18. The calculated reflectivity spectrum shows no dip near ω_{LO}, but does show a flattened region near 385 cm^{-1}, in good agreement with the experimental results of Fig. 17.

The Raman spectrum of GaP doped with Mg is very similar to the case of Zn[14,19] showing a broad peak similar to *C* in Fig. 18(a). No reflectivity dip was observed in the present infrared study. Rough fits similar to those described above show that the Raman spectrum can be reproduced and the negative infrared result explained. Again it is the broad damped nature of the Mg acceptor transitions which prevents the formation of a sharp localized LO resonance. It is interesting to note that in both these cases where $0.75E_B \sim \hbar\omega_{\mathrm{LO}}$ not only does the electronic transition perturb the phonons, but the phonons perturb the electronic transition. For the case of Zn, we identify the peak at 450 cm^{-1} in the Raman spectrum as the electronic transition. The "zero-order" transition required by the model must be placed at 390 cm^{-1}, thus illustrating the strong electron-phonon interaction.

The Cd acceptor in GaAs (Table II) and the Be acceptor in GaP also showed no reflectivity dip, probably for the same reasons outlined above. The Ge acceptor in GaAs is somewhat more favorable than the Cd acceptor since it has a higher E_B. For the Ge acceptor the low-temperature reflectivity spectrum showed a slight dip 5 cm^{-1} below ω_{LO}. We believe this represents the localized mode. The hole concentration at 300 K was 3×10^{17} cm^{-3}. Because of the noise level involved in this run better confirmation would require samples with concentrations at least twice as large.

Finally, for *C* acceptors in GaP a sharp but weak dip was found 6 cm^{-1} below ω_{LO}. Since E_B is quite small (48 meV), this case appears unfavorable for the formation of a sharp local mode for the same reasons as discussed above for GaP: Zn. The explanation for the sharp mode observed may be that the lowest acceptor transition is well below ω_{LO}. Higher-lying transitions could provide a positive dielectric constant $\epsilon_{el} \sim 7$ near ω_{LO} which causes a localized phonon in the usual manner. The lowest transition in this case must be under the ω_{LO} bulk phonon and would be hard to detect. More Raman and infrared transmission spectroscopy is needed to confirm this explanation.

In conclusion, a new type of localized mode has been observed for the first time in infrared spectra. The mode results from the interaction of the polar optical lattice vibrations and a low-lying electronic transition. The classical macroscopic model developed above gives a useful picture of the mode. The model can be used to predict both Raman and infrared strengths for the local mode and forms a basis for making more detailed comparisons with a quantum theory of the electronic transitions.

ACKNOWLEDGMENTS

The author is indebted to D. D. Manchon for permission to use his unpublished Raman spectra and to B. I. Halperin and J. J. Hopfield for critical discussions on the sphere model. It is a pleasure to acknowledge the capable experimental work of J. A. Ditzenberger. M. Ilegems, M. Weiner, and H. W. Verleur kindly supplied most of the samples studied.

---

[1]G. Schaefer, J. Phys. Chem. Solids **12**, 233 (1960).

[2]For theoretical and experimental reviews on localized vibrational modes see A. A. Maradudin, in *Localized Excitations in Solids*, edited by R. F. Wallis (Plenum, New York, 1968), p. 1; A. J. Sievers, in *Localized Excitations in Solids*, edited by R. F. Wallis (Plenum, New York, 1968), p. 27.

[3]P. J. Dean, D. D. Manchon, Jr., and J. J. Hopfield, Phys. Rev. Lett. **25**, 1027 (1970).

[4]A. S. Barker, Jr., Bull. Am. Phys. Soc. **16**, 311 (1971).

[5]In GaP the primitive ion-pair volume is 40.5×10^{-24} cm^3. Taking the cube root, $a_0 = 3.43$ Å.

[6]L. D. Landau and E. M. Lifshitz, *Electrodynamics of Continuous Media* (Pergamon, Oxford, 1960), Sec. 7.

[7]The reader is reminded that a medium characterized by a dielectric function ϵ_{gas} has transverse-optic modes (for wave vector k much greater than ω/c) at frequencies where ϵ_{gas} has poles and longitudinal-optic modes at frequencies where ϵ_{gas} has zeros.

[8]In practice the dielectric function is complex so that resonance conditions such as Eqs. (9)–(11) and (13) have a solution only for a complex frequency. The real part of the resonance condition usually yields a real frequency which is close to the location of the peak in the measured response. It must be emphasized that a detailed comparison with experiments requires the full response function such as Eq. (8) or Eq. (12) and not just a resonance condition.

[9]H. Frohlich, *Theory of Dielectrics*, 2nd ed. (Clarendon, Oxford, 1958), Sec. 18.

[10]Formulas of this type were used long ago to explain the conductivity of solid mixtures: Lord Rayleigh, Philos. Mag.

34, 481 (1892); also R. Landauer, J. Appl. Phys. **23**, 779 (1952). The present formula [Eq. (12)] has recently been derived independently by L. Genzel and T. P. Martin, Phys. Status Solidi **51**, 91 (1972), and by F. L. Galeener, Phys. Rev. Lett. **27**, 421 (1971).

[11]W. Cochran, Z. Kristallogr. **112**, 465 (1959); also A. S. Barker, Jr., Phys. Rev. 136, A1290 (1964).

[12]W. G. Spitzer and D. A. Kleinman, Phys. Rev. **121**, 1324 (1961).

[13]A. S. Barker, Jr., Phys. Rev. **165**, 917 (1968).

[14]D. D. Manchon (unpublished). See also D. D. Manchon and P. J. Dean, in *Proceedings of the Tenth International Conference on the Physics of Semiconductors* (U. S. AEC, Oak Ridge, Tenn., 1970), p. 760.

[15]This suggestion was first made by D. D. Manchon and P. J. Dean (unpublished).

[16]N. F. Mott and I. N. Sneddon, *Wave Mechanics and Its Applications* (Clarendon, Oxford, England, 1948), Sec. 32.

[17]The correct treatment of the polarizability of a bound charge in a dielectric with dispersion is extremely complicated and parameter sensitive even in the continuum model. See, for example, J. J. O'Dwyer and H. H. Nickle, Phys. Rev. B **2**, 5063 (1970).

[18]A. S. Barker, Jr. and R. Loudon, Rev. Mod. Phys. **44**, 18 (1972).

[19]C. H. Henry, J. J. Hopfield, and L. C. Luther, Phys. Rev. Lett. **17**, 1178 (1966).

[20]A. S. Barker, Jr. (unpublished).

PHYSICAL REVIEW B VOLUME 7, NUMBER 6 15 MARCH 1973

Alfvén-Wave Propagation and Damping in Pyrolytic and Single-Crystal Graphite*

Alan R. Krauss† and Jacek K. Furdyna
Department of Physics, Purdue University, Lafayette, Indiana 47907
(Received 6 July 1972)

A systematic study of Alfvén-wave propagation was carried out at 35 GHz in pyrolytic and single-crystal graphite by means of microwave transmission and reflection experiments at 4.2 and 77 K. The amplitude and phase of the propagating wave were measured independently, yielding values of the collision frequency and the effective-carrier mass density at 4.2 K. These values were in reasonable agreement with theoretical and previously reported experimental values, although there was some evidence that the collision time is magnetic field dependent. The measured mass densities for pyrolytic and single-crystal samples were the same within experimental error. Transmission measurements were carried out as a function of angle between the applied magnetic field and the direction of propagation, revealing a quasi-two-dimensional behavior of the mass density, characteristic of graphite. On the other hand, these measurements indicate little anisotropy in the scattering rate. Experiments performed at 77 K yield a slightly higher value of the mass density, in agreement with the nonparabolic energy-band structure predicted by the Slonczewski–Weiss model. Very pronounced oscillatory structure observed in Alfvén-wave damping at 4.2 K in the case of single-crystal graphite is identified as Shubnikov–de Haas oscillations associated with *both* majority and minority carriers. The single-crystal data also revealed a small oscillation in the transmitted phase.

I. INTRODUCTION

Semimetals with equal electron and hole concentrations (such as bismuth, antimony, and graphite) are capable of supporting wave propagation of a type similar to that described by Alfvén[1] for two-component gaseous plasmas. The first direct observations of Alfvén-wave transmission in solids were made by Williams[2] for bismuth and antimony by detecting the interference between microwave leakage around the sample and transmission through the sample. Transmission-amplitude measurements have been used to determine collision frequencies in bismuth and the transmission envelope has exhibited Shubnikov–de Haas oscillations in damping.[3] The transmitted phase has also displayed Shubnikov–de Haas effects due to variation in carrier concentration.[4]

In comparison with bismuth, graphite has received relatively little attention. Because of its greater carrier concentration and higher collision frequency (both are an order of magnitude larger), graphite is considerably less transparent, requiring either very high fields, thin samples, or sensitive apparatus to detect transmission. However, the constant-energy surfaces of the carriers in graphite are parallel to a common symmetry axis and the effects associated with Fermi-surface anisotropy are considerably simplified. Graphite is therefore a material of interest in the study of electromagnetic-wave propagation in compensated solids.

Alfvén waves were first observed in graphite by Surma, Furdyna, and Praddaude[5] by means of geometric interference in a thin flake mounted inside a microwave reflection cavity. The experimental geometry was that of the "fast" Alfvén wave, i.e., the plane of polarization (direction of $\vec{E}_{rf}$) was perpendicular to both the dc magnetic field and wave vector $\vec{q}$, and the magnetic field